

Affinity of Sulfamates and Sulfamides to Carbonic Anhydrase II Isoform: Experimental and Molecular Modeling Approaches

Luciana Gavernet,^{*,†} Jose L. Gonzalez Funes,[†] Luis Bruno Blanch,[†] Guillermina Estiu,[‡]
Alfonso Maresca,[§] and Claudiu T. Supuran[§]

Medicinal Chemistry, Department of Biological Sciences, Faculty of Exact Sciences, National University of La Plata, 47 and 115, La Plata B1900BJW, Argentina, Walther Cancer Research Center and Department of Chemistry and Biochemistry, University of Notre Dame, Notre Dame, Indiana 46556-5670, and Università degli Studi di Firenze, Polo Scientifico, Laboratorio di Chimica Bioinorganica, Rm. 188, Via della Lastruccia 3, 50019 Sesto Fiorentino (Florence), Italy

Received March 23, 2010

Sixteen aromatic and aliphatic sulfamides and sulfamates were synthesized and tested in their inhibition to carbonic anhydrase CAII activity. The weaker inhibition pattern shown by sulfamides as compared to sulfamates is interpreted in this research by means of molecular modeling techniques, including known inhibitors (topiramate and its sulfamide cognate) in the analysis. The results nicely explain the origin of the inhibitory activity, which is not only related to positive interactions of the ligand with the active site residues but also to the solvation pattern characteristic of each ligand.

INTRODUCTION

Carbonic anhydrases (CAs) comprise a family of zinc metalloenzymes that catalyze the reversible hydration of carbon dioxide to bicarbonate ion.^{1–6} The assistance for the rapid interconversion between these two species has an important effect on some vital physiological as well as pathologic processes. Most of the CA enzymes have been characterized in detail, and classified in five distinct gene families: α -, β -, γ -, δ -, and ξ -CA families.⁷

Sixteen α -CA isoforms have been isolated in mammals with different subcellular localization and tissue distribution. In all cases, the catalytic site consists of a Zn (II) ion tetrahedrally coordinated by the imidazole rings of three histidine residues (His94, His96, and His119, PDB code 2H15),⁷ with the fourth position occupied by a water molecule at an acidic pH (<8) and by a hydroxide ion at a higher pH.^{1–6} Due to the important role of α -CAs in higher vertebrates, the study of these enzymes represents an attractive target for the design of inhibitors and activators with therapeutic value. Compounds possessing CA inhibitory properties have been utilized as anticonvulsant, antirolithic, antiglaucoma, and anticancer agents.⁷ In terms of their structural characteristics, most of the inhibitors possess a zinc binding function capable of substituting the nonprotein zinc ligand.⁷

Human CAII (hCAII) is the physiologically most relevant and widespread CA isoform. It is also the most extensively studied from structural and inhibitor design points of view and is a benchmark in molecular dynamics simulations.^{8–11} Computational three-dimensional (3D) quantitative structure–activity relationship (QSAR) and virtual screening

strategies have been used to search for new inhibitors.^{12–15} Nevertheless, the most potent inhibitors used in clinic (acetazolamide, methazolamide, ethoxzolamide, dichlorophenamide, dorzolamide, brinzolamide) still present a primary sulfonamide group on a benzenic or heterocyclic structure that binds to the zinc ion through the deprotonated nitrogen atom.^{4–7} Whereas this group is recognized as the most frequent anchoring group in CAII, other closely related functions have shown promising inhibitory action. This is the case of the new generation anticonvulsant drug topiramate (TOP, a sugar sulfamate, Figure 1) as well as several related compounds like its 4,5-cyclic sulfate congener (compound **3**, Figure 1, TOP-like).¹⁶ TOP shows good activity in CA inhibition, at variance with its sulfamide cognate (STOP, compound **2**, Figure 1), which exhibits a weak inhibitory action.¹⁶ The different activity of sulfamates and sulfamides in CAII inhibition has been discussed in the literature¹⁶ as well as the larger potency of aryl than alkyl sulfamides.¹⁷ Nevertheless, the differences in the sulfamate/sulfamide CAII inhibitory activity reported for topiramate and related structures exceed the values characteristic of simpler alkyl and aryl ones, pointing to an influence of the nonbinder portions of the inhibitor in modulating the activity through interactions with protein residues and/or indirectly impacting the pK_a of the ligand.

Following previous research in this line, we decided to investigate in some detail the different effects that can contribute to the trend observed in the sulfamide/sulfamates CAII activity. To this end, we synthesized and tested several *N*-substituted and *N,N'*-disubstituted alkyl and aryl sulfamides (Figure 1) and analyzed their interactions in the CAII active site using molecular modeling techniques. From this set, representative structures of alkyl and aryl sulfamides as well as their cognate sulfamates were selected for further analysis. Extensive molecular dynamics simulations of *N*-butyl, *N,N'*-dibutyl, *N*-benzyl, *N,N'*-dibenzyl, *N*-cyclohexyl and *N,N'*-dicyclohexyl-sulfamide,

* Corresponding author. Telephone: +54 0221-4235333. Fax: +54 02214223409. E-mail: lgavernet@biol.unlp.edu.ar.

[†] National University of La Plata.

[‡] University of Notre Dame.

[§] Università degli Studi di Firenze.

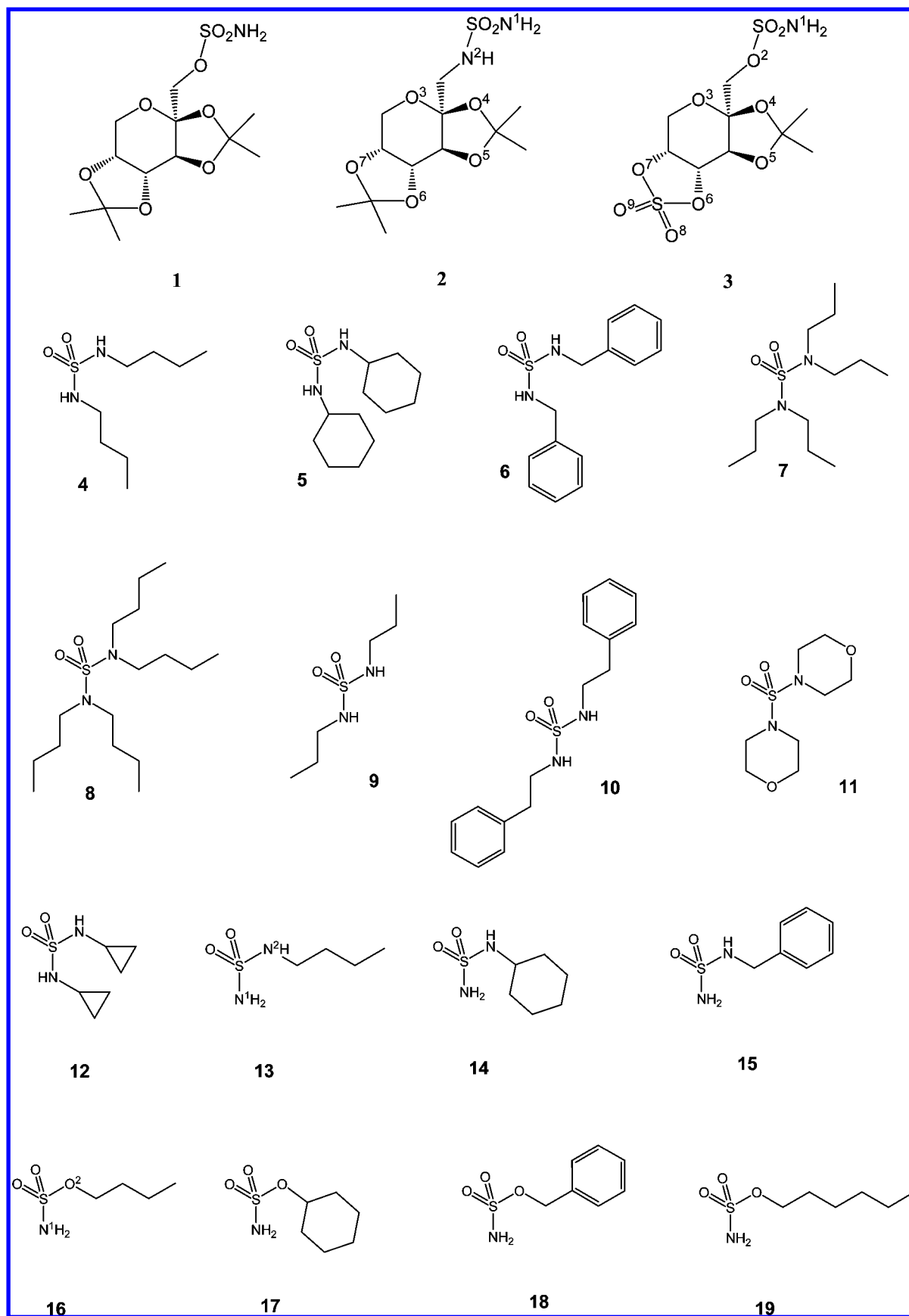


Figure 1. Chemical structures of the compounds analyzed in this investigation. **1:** topiramate, **2:** topiramate sulfamide analogue, **3:** topiramate cyclic sulfate analogue. Sulfamides **4–12** and sulfamate **19** were synthesized and tested by some of us. Inhibitory activity of compounds **13–18** was taken from literature.

STOP, and their cognate sulfamates have been used to analyze the interactions with residues and solvent waters of the active

site pocket that can modulate the pK_a of the ligand and the consequent strength of the binding.

EXPERIMENTAL SECTION

The sulfamides/sulfamates were prepared as mentioned in literature.^{18–20} Their synthesis, characterization, and identification have been already reported by some of us in preceding investigations.^{18–20} Sulfamides **4–12** were prepared by condensation of an excess of the corresponding amine with sulfuryl chloride,^{18,19} whereas monosubstituted sulfamide **15** was obtained by acidic hydrolysis of its *N*-alkoxycarbonyl sulfamide derivative, the *N*-(benzyl)-*N'*-(*tert*-butoxycarbonyl)sulfamide.¹⁹ This derivative was synthesized using chlorosulfonyl isocyanate, *tert*butanol, and the benzylamine in the presence of triethylamine. Sulfamate **19** was prepared by adding formic acid to chlorosulfonyl isocyanate to generate sulfamoyl chloride, which was then allowed to react in situ with hexyl alcohol in the presence of pyridine.

Compounds **13–14** and **16–18** were not synthesized. Their biological information was taken from literature.

CA Inhibition. An applied photophysics stopped-flow instrument has been used for assaying the CA-catalyzed CO₂ hydration activity.²¹ Phenol red (at a concentration of 0.2 μM) has been used as an indicator, working at the absorbance maximum of 557 nm, with 20 mM of Hepes (pH 7.4) and 20 mM of NaBF₄ (for maintaining constant the ionic strength), following the initial rates of the CA-catalyzed CO₂ hydration reaction for a period of 10–100 s. The CO₂ concentrations ranged from 1.7 to 17 μM for the determination of the kinetic parameters and the inhibition constants. For each inhibitor, at least six traces of the initial 5–10% of the reaction have been used for determining the initial velocity. The uncatalyzed rates were determined in the same manner and subtracted from the total observed rates. Stock solutions of inhibitor (10 μM) were prepared in distilled deionized water, and dilutions up to 0.01 μM were done thereafter with distilled deionized water. Inhibitor and enzyme solutions were preincubated together for 15 min at room temperature prior to assay, in order to allow for the formation of the E–I complex. The inhibition constants were obtained by nonlinear least-squares methods using PRISM 3, whereas the kinetic parameters for the uninhibited enzymes were from Lineweaver–Burk plots, as reported earlier,^{22,23} and represent the mean from at least three different determinations.

Computational. Docking. Binding of the compounds, shown in Figure 1, was analyzed using AutoDockTools 1.5.0 and AutoDock 4.0 docking programs.²⁴ The starting protein was prepared from the 0.99 Å resolution crystal structure of the CAII–sulfonamide complex deposited by Christianson et al (PDB code 2FOU).²⁵ We have chosen the highest-resolution CAII crystal structure from the Protein Data Bank (PDB code 2FOU) accepting that CAII possess a low degree of movement upon the binding of different ligands.¹⁴ Only for the cases of STOP, TOP, and TOP-like, the cocrystallized structures were used, namely 2H15, 3HKU, and 1EOU, respectively. In all cases, the crystallographic water molecules, the ligand, and any cocrystallized molecule/ion were stripped. Hydrogen atoms were added using the leap module of AMBER9.²⁶ Special attention was given to the protonation states of the His residues of the active site that were defined as HID94, HID96, and HIE119.

We used the default Autodock parameters for all the variables but the charges of the ligands, for which AM1-BCC charges were calculated using quacpac.²⁷ We found this performs better in the docking for this particular system than the default Gasteiger charges.

The structures were docked using the Lamarckian genetic algorithm (LGA) in the “docking active site”, defined through a grid centered on the N atom of the ASN67 residue of CAII (coordinates: X = 3.766, Y = 1.766, Z = –9.060), with 60, 50, and 60 grid point in X, Y, Z dimensions, respectively. We use the default grid spacing (0.375 Å) and performed 50 docking runs, treating the docking active site as a rigid molecule and the ligands as flexible, i.e., all nonring torsions were considered active. The compounds were docked in their deprotonated form when possible. Exceptions were compounds **7**, **8**, and **11** bearing no H attached to the binding N and compound **2** for which several protonation states were analyzed.

For the particular case of STOP the conformational space of the ligand was explored by a Macromodel²⁸ conformational search using the Monte Carlo multiple search algorithm with the OPLS-2005 force field,²⁹ followed by further structural clustering according to the heavy atoms root-mean-squared (rms) value (XCluster).³⁰

Molecular Dynamics. The conformations predicted by Autodock were used as starting points for molecular dynamics (MD) simulations, with the exception of **5** for which the docking did not give any good pose, in agreement with the low inhibitory activity observed for this molecule. For that reason, we built the initial structure using, as a template, the conformation obtained from the docking of **6**. In case of STOP, TOP, and TOP-like, we use their corresponding cocrystallized structures as starting points.

MD simulations were carried out using the PMEMD version included in the AMBER10 suite of programs,³¹ after careful relaxation of the system using minimization and equilibration protocols. The initial geometries were minimized (1000 cycles for the water molecules followed by 2500 cycles for the entire systems). After a 20 ps NTV equilibration period with a weak restraint (10 kcal/mol Å²) for the complex and a NTP 200 ps without restraint, production runs larger than 12 ns were computed for each complex, for the coordinates saved every 1000 time steps.

The ionizable residues were set to their normal ionization states at pH 7, except for the HIS residues coordinating the Zn metalcenter, which were modeled as HID94, HID96, and HIE119. The protein atoms as well as all the water molecules of the crystal structure were surrounded by a periodic box of TIP3P³² water molecules that extended 10 Å from the protein. Na⁺ counterions were placed by LEaP²⁶ to neutralize the system.

The ff03 version of the all-atom AMBER force field was used to model the protein, and the GAFF force field was used for the organic ligand.³³ Atom-centered partial charges were derived by using the AMBER antechamber program (restrained electrostatic potential [RESP] methodology),^{34,35} after geometry optimization at the B3LYP/6-31G* level.³⁶ Nonstandard force fields have been derived for the Zn active site by means of geometry minimization (B3LYP/6-31G**, G03),³⁷ followed by calculation of the second derivatives and RESP charges for the active site supermolecule defined by three His residues, the Zn ion, and the sulfamide ligand.

Table 1. Biological Activity, Docking Scores, and Relevant Geometric Data Derived from the Docking^a

compound	K_i (μ M)	K_i ratio	score	$d1$ (\AA)	$d2$ (\AA)	rms fit
1	0.01 ¹⁶		-6.63	1.66	3.89	0.546
2 (STOPZ)	2.135 ¹⁶	213.5	-4.83	1.43	2.51	0.381
2 (STOPN)	2.135 ¹⁶	213.5	-6.84	1.57	2.08	0.612
3	$IC_{50} = 36$ ¹⁶		-5.76	1.58	1.96	0.427
4 ¹⁸	66.3		-4.87	1.72		NA
5 ¹⁸	100.1		-			NA
6 ¹⁸	0.65		-4.86	1.70		NA
7 ¹⁹	>200		-			NA
8 ¹⁹	>200		-			NA
9 ¹⁹	124		-5.37	1.77		NA
10 ¹⁹	>200		-			NA
11 ¹⁹	135		-			NA
12 ¹⁹	>200		-4.6	1.62		NA
13 ¹⁹	0.148 ¹⁷	2.1	-5.43	1.60	2.00	NA
14 ¹⁹	0.45 ¹⁷	7.5	-5.78	1.58	1.98	NA
15 ¹⁹	0.123	36.2	-6.64	1.59	1.95	NA
16	0.07 ⁴³		-5.39	1.58	3.54	NA
17	0.06 ⁴³		-6.3	1.58	1.99	NA
18	0.0034 ⁴³		-6.25	1.59	1.97	NA
19 ²⁰	2.82		-5.56	1.60	1.91	NA

^a The references of the biological data published before as well as the references for the preparation of the compounds are indicated as superscripts in the table. K_i ratio: K_i of sulfamides relative to the K_i of its respective cognate sulfamate. NA: x-ray structure not available. $d1$: Zn–N¹ distances derived from the docking. c - $d2$: Calculated N¹H–OG1THR199 distances derived from docking. RMSfit: root mean square for the superimposition of the experimental and the docking conformation.

Different force fields were derived for mono- and disubstituted sulfamides, considering (His)₃Zn–N¹H¹–SO₂–NH₂ and (His)₃Zn–N¹(CH₃)–SO₂–NH₂ coordination motifs. In the MD simulation protocol, the time step was chosen to be 2 fs, and the SHAKE algorithm³⁸ was used to constrain all bonds involving hydrogen atoms. A nonbonded cutoff of 10.0 \AA was used, and the nonbonded pair list was updated every 25 time steps. Langevin dynamics was used to control the temperature (300 K) using a collision frequency of 1.0 ps⁻¹, with isotropic position scaling to maintain the pressure (1 atm).³⁹ Periodic boundary conditions were applied to simulate a continuous system. To include the contributions of long-range interactions, the particle mesh Ewald (PME)^{40,41} method was used with a grid spacing of ~ 1 \AA combined with a fourth-order B-spline interpolation to compute the potential and the forces in between grid points. The trajectories were analyzed using the PTRAJ module of AMBER.

RESULTS

Table 1 shows the biological activity determined for the compounds shown in Figure 1.

The weaker inhibition pattern of sulfamides compared to sulfamates is in agreement with previous results reported for similar structures.^{17,42,43} The scores predicted by the Autodock docking are also given in Table 1, column 4, and relevant calculated distances involved in Zn binding are shown in columns 5 and 6. The N atoms in the sulfamide function are referred to as N¹ for the N atom coordinated to Zn in the active site of CAII and N² for the noncoordinating N atom that bears the substitution (as exemplified for compounds **2**, **3**, **13**, and **16** in Figure 1). For the sulfamide

analogue of TOP, three different protonation states have been considered: the neutral structure (STOPH), the deprotonated form (STOPN), and a “zwitterion” conformation that involves a negative coordinating N¹ and a positive noncoordinating N² (STOPZ).

Autodock is capable of predicting the binding disposition of STOP, TOP, and TOP-like with rms fit errors from 0.4 to 0.6 (Table 1) relative to the respective crystallographic structures (2H15 for STOP, 1EOU for TOP-like, and 3HKU for TOP), which increase our confidence in the predicted binding conformation of the other compounds (see Supporting Information, Figure S1). The error is smaller in the STOPZ fit as compared to STOPN. On the other hand, no good coordination was attained for the neutral structure (STOPH). Figure 2 shows representative binding geometries for *N*-substituted sulfamides, *N,N'*-disubstituted sulfamides and sulfamates, as they result from the docking. STOP, TOP, and TOP-like are shown in Figure 3.

The binding reproduces the X-ray determined interactions of the zinc-binding function, stabilizing a H bond between the THR199 OG and the H atom of the N¹ of the sulfamide group. In the single *N*-substituted sulfamides and sulfamates (compounds **13**–**19**, Figure 1), the interaction is reinforced by a H bond comprising the backbone NH of the same residue and the O of the sulfonyl group of the ligand. STOP also displays similar H-bond interactions with THR199 and THR200, adding interactions of the O-atoms of the organic scaffold with ASN62 and GLN92. All of them are well reproduced by the docking as well as the negative van der Waals contacts between one methyl group of STOP and its nearest residues (the side chain of ALA65 and the carboxamide group of ASN67), previously discussed in the literature as a possible reason for its low inhibitory activity.¹⁶ The same holds for TOP-like and TOP, where the docking perfectly resembles the interactions with THR199, THR200, ASN62, and GLN92. The docking procedure also detects the different orientation of these two related compounds in the binding site. The molecules are rotated around the anomeric C–CH₂ bond relative to each other, and the 2,3 ring of one ligand has exchanged positions with the 4,5 ring of the other ligand.

No good coordination was achieved for the case of the nonactive compounds, **5**, **7**, **8**, **10**, and **11**, which bear sizable substituents on N¹. Substitution in N¹ also impairs the activity of **4** and **5** relative to the single-substituted analogs and is reflected in a lower score. No H-bond interaction with the THR199 OG can be established in this case, and only the acceptor properties of the sulfamide sulfonyl O can add to the stabilization (Figure 2C and D).

The different activity of sulfamides and sulfamates is not well reproduced by the docking algorithms (compare compounds **13** and **16**, Table 1), as the calculation of the binding energy value considers the coordination of the negative species to the Zn active site, i.e., the different p*K*_a is not accounted for in the docking score. Even though the p*K*_a can be relevant in determining the different activity, it does not seem to be enough to justify the K_i ratio of STOP/TOP, two orders of magnitude larger than that of **13/16**. Among the different possible justifications discussed in the literature, a steric clash of the methyl substituent of one of the dioxolane rings of STOP with ALA65 has been mentioned. This group is also present in TOP but has a slightly different orientation

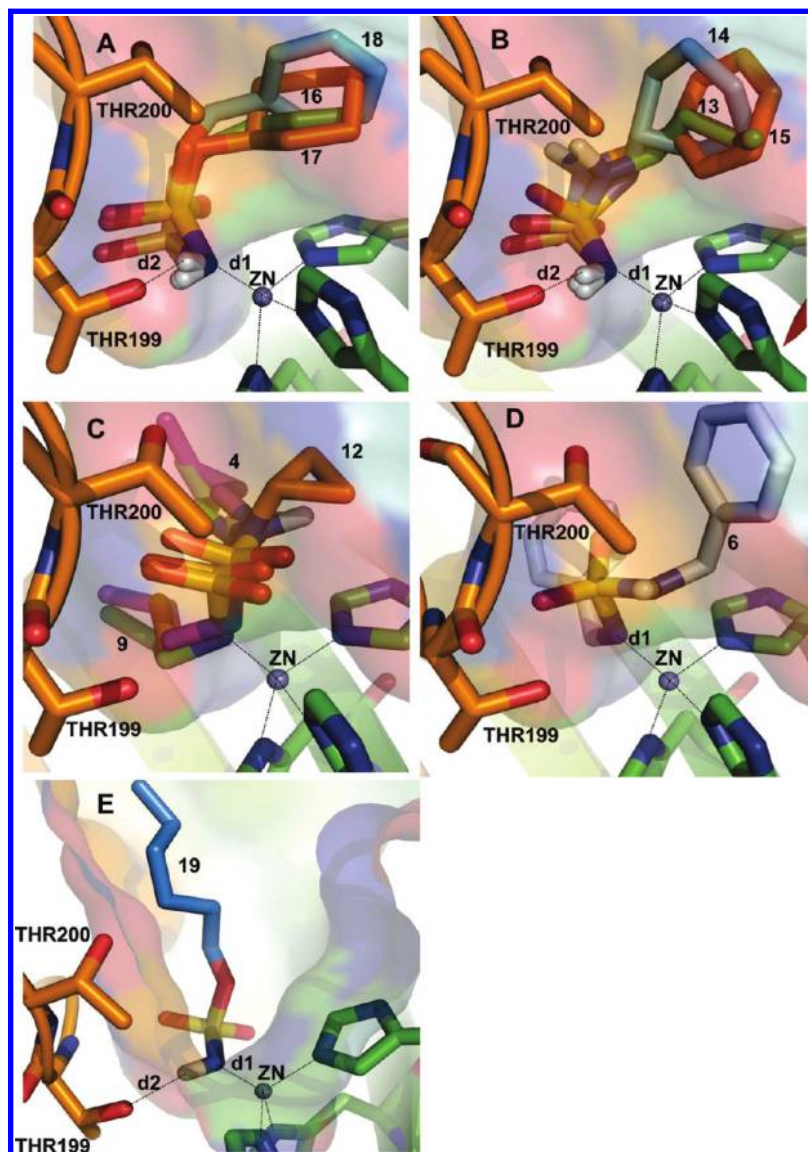


Figure 2. Binding geometries of compounds 4–19 in the CAII active site predicted by the Autodock docking algorithms. Histidine residues of the active site are highlighted in green, and THR199 residue is highlighted in orange. Zn atom is represented as a nonbonded sphere in gray. Only H atoms attached to N of the ligand are shown. Values of the relevant distances named as $d1$ and $d2$ are given in Table 1. For clarity, carbon chains of the ligands are represented in different colors: (A) monosubstituted sulfamates **16** (green), **17** (orange), and **18** (light blue); (B) monosubstituted sulfamides **13** (green), **14** (light blue), and **15** (orange); (C) Disubstituted sulfamides **4** (violet), **9** (green), and **12** (orange); (D) compound **6** (white); and (E) Compound **19** (blue).

that prevents this negative interaction. The compounds only differ in the bioisosteric substitution of O by NH, which is enough to trigger a different orientation of the dioxolane rings as the S–X–C angle (X = O, N) changes from 122 to 111 as X changes from O to NH. In this way, different intra- and intermolecular interactions in the active site pocket can be stabilized in both cases.

To assess the molecular basis of the differences observed in the affinity of sulfamates and sulfamides toward hCA II, 12 ns MD simulations were carried out for butyl, benzyl, and cyclohexyl-sulfamates and sulfamides as representative of aliphatic, cyclic, and aromatic-substituted species. The analysis was extended to the case of TOP and STOP as a way of testing the credibility of the results through the comparison with experimental data. TOP was modeled by its analog TOP-like as no X-ray structure was available when the simulations were run. For the case of STOP, different protonation states have been considered (see Experimental

Section) to better account for the possible reasons for the large fold difference (Table 1). The H-bond interaction pattern connecting the ionized N¹H group to THR199OG is kept for both *N*-butyl sulfamide and *N*-butyl sulfamate over the 12 ns MD runs with average distances of 2.16 and 2.05 Å, respectively. The binding is further stabilized by the interaction of a sulfonyl O accepting a H from either the THR200 HG or the THR199 H in an oscillating manner. The aliphatic tail shows a similar orientation in both cases, pointing toward the hydrophobic part of the active site pocket; resembling the pattern shown in the crystallographic structures of aliphatic sulfamates.⁴⁴

The bioisosteric substitution of O by N²H does not impact the interactions of the binder group in the CAII active site. Nevertheless, striking differences become evident when the interactions of the surrounding solvent water molecules are considered. A solvent water molecule is always donating an H atom to the N¹H group of the sulfamide throughout the

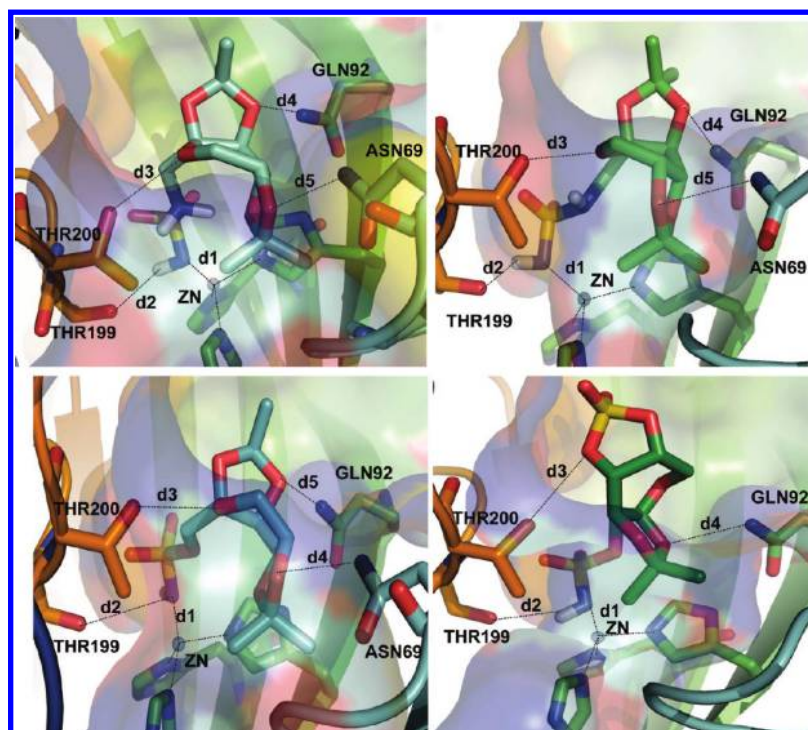


Figure 3. Binding geometries of compounds 1–3 in the CAII active site predicted by the Autodock docking algorithms. HIS residues of the active site are highlighted in green, and THR residues are highlighted in orange. Zn atom is represented as a nonbonded sphere in gray. Only H atoms attached to N of the ligand are shown. Values of the relevant distances named as $d1$ and $d2$ are given in Table 1. (A) STOP in its “zwitterion” conformation (STOPZ). Other significant distances are: $d3 = 3.17$, $d4 = 2.27$, and $d5 = 3.10$ Å. (B) STOP in its deprotonated conformation (STOPN). Other significant distances are: $d3 = 3.39$, $d4 = 2.66$, and $d5 = 3.45$ Å. (C) TOP. Other significant distances are: $d3 = 3.03$, $d4 = 2.49$, and $d5 = 2.95$ Å. (D) TOP-like. Other significant distances are: $d3 = 3.45$ and $d4 = 3.45$ Å.

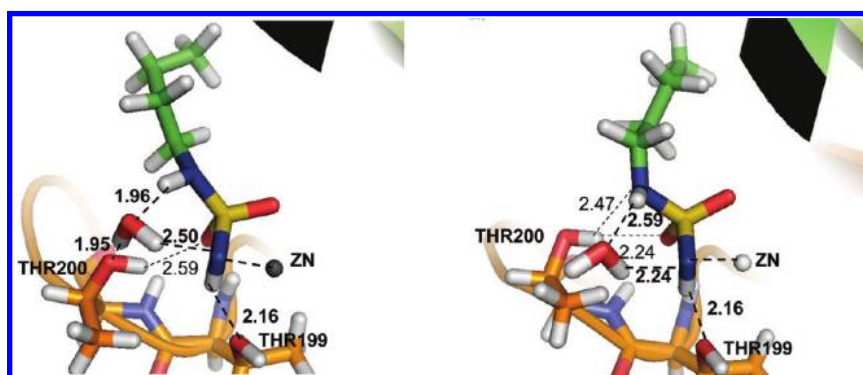


Figure 4. Representative snapshot that shows the interaction of butyl sulfamide with water molecules. The distances (in Å) correspond to average values.

simulation, while the water O atom is the acceptor of a H-bond coordination with the sulfamide N^2H . THR200 is also involved in this coordination alternating between OG–water and HG– N^2 interactions (Figure 4). Water molecules also diffuse when the active site pocket is occupied by a sulfamate, but the solvent donates its H to the sulfamate O. Representative snapshots are shown in Figures 4 and 5. The coordination of a water H atom compromises the lone pair electrons of the Zn– N^1 atom, significantly impairing the coordination capability to the metal center.

Similar interactions with Zn, THR199, and THR200 stabilize the binding of *N*-benzyl sulfamide and *N*-benzyl sulfamate, and a similar solvation pattern can be described (see Supporting Information, Figure S2). There are no differences in the solvation pattern or in the coordination with THR199 and THR200 for the cyclohexyl substitution (see Supporting Information, Figures S3).

Neither THR199 nor THR200 participates directly in stabilizing the binding of the *N,N'*-disubstituted sulfamides. The N^2 atom can H bond a solvent water molecule and partially interact through it with THR199. Another solvent molecule can also reach deep into the pocket and H bond, the N^1 atom of *N,N'*-dibutylsulfamide. This interaction is not as stable as in the single-substituted counterpart and is not found in the simulation of the CAII–*N,N'*-dibenzylsulfamide system. *N,N'*-disubstitution markedly impairs the activity as it impedes important H-bond stabilizations of the binder sulfamide group in the bottom of the active site pocket. The effect is less evident for the case of the aromatic benzyl substituent, as a partial π -stacking between the phenyl rings reinforces the electronic density and, hence, a T-shape interaction with PHE150 (see Supporting Information, Figure S4).

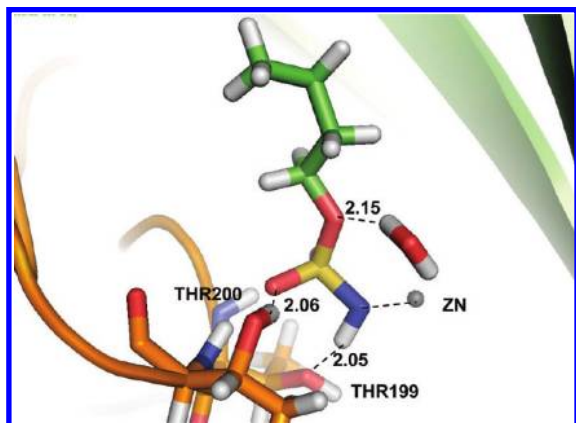


Figure 5. Representative snapshot that shows the interaction of butyl sulfamide with water molecules. The distances (in Å) correspond to average values.

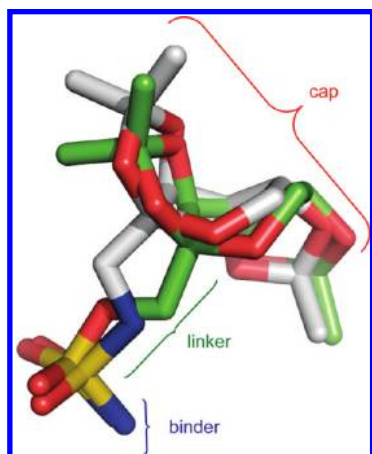


Figure 6. Superimposition of STOP and TOP from the cocrystallized structures 2H15 (STOP) and 3HKU (TOP).

There is no diffusion of solvent molecules into the CAII active site pocket bound to bulky ligands as TOP-like or STOP in the course of 12 ns MDs, which makes it even more difficult to justify their K_i ratio. A thorough comparison of the cocrystallized CAII–TOP (3HKU) and CAII–STOP (2H15)⁷ has pointed out minor differences in the interactions with the residues of the active site pocket, mainly focusing in the H-bond interactions of the endocyclic sugar oxygens and clashes of the methyl substituent of the dioxolane rings with ALA65, which can be avoided in the case of TOP. Although the cocrystallized ligands can be nicely superimposed in the binder and sugar cyclic moieties (cap), they differ in the spatial orientation of the O/NH linker (Figure 6). The spatial orientation of the cap is, hence, more conserved among similar ligands than the conformation of the linker, showing that a different orientation would be disfavored. Nevertheless, the different linker determines the small differences in the fitting of the cap in the active site pocket that have been pointed out as relevant in impairing the activity.

Neither the O in TOP nor the N²H in STOP in the linker region participates in any interaction with protein residues. STOP N² is, however, 2.76 Å from the endocyclic sugar O (named as **3** in Figure 1) and 3.21 Å from the O6 atom of one dioxolane ring, suggesting a H-bond coordination of N² with at least one of these O atoms. In order to discern the protonation state and possible intramolecular H-bond interactions of the STOP molecule cocrystallized with CAII, we

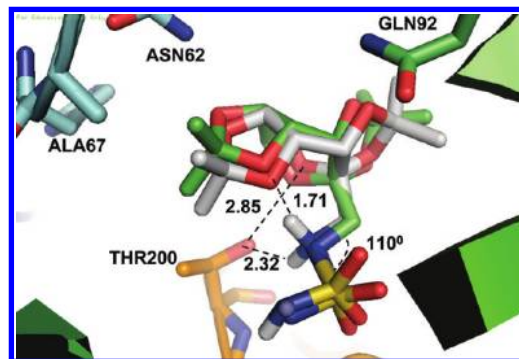


Figure 7. Coordination of STOPZ (carbon atoms in white) in the CAII active site resulting from conformational search. The X-ray structure (2H15) is shown (carbon atoms in green) for comparison. More details in the text.

performed an exhaustive conformational search for the different possible protonation states of STOP, neutral (STOPH), deprotonated (STOPN), and the “zwitterion” (STOPZ) that can be formed by proton transfer in the event of the docking. We found the best agreement to the experiment for the zwitterionic conformation (Figure 7). Only this isomer reproduces the 111° value of the S–N–C angle of STOP (110.2° calculated) which is compatible with a sp³ hybridization of the N atom. The resulting bound conformation is stabilized through the formation of two H bonds: a N²–H–O bond with one dioxolane O6 acting as acceptor and a second N²–H–OG reinforced by coordination of HG to the STOP O3 (Figure 7). It also reproduces the interactions of the sulfamide binder with THR199 and THR200 and the H-bond interaction network of the cap with near neighbor residues. As previously mentioned, no good coordination was attained for the neutral structure (STOPH), and the rms values obtained from superimposition of the docked conformations of STOPN and STOPZ (Table 1) with the crystallographic conformation of STOP confirmed that STOPZ better models the cocrystallized structure.

In order to better understand if the STOPZ conformation can be formed through an assisted proton transfer between the STOP N atoms, we repeated the conformational search modeling an explicit water molecule close enough to STOP to stabilize a STOP–water ensemble. The lowest conformation that results from the search features the water molecule accepting a H from N¹H₂ and establishing a bifurcated H bond with the second Stop N atom and the pyranose O3, enabling the proton transfer that leads to STOPZ. The superposition of the STOP–water supermolecule with 2H15 shows the water molecule playing the role of THR200 in H-binding O3, suggesting a possible N¹–OG–O3 H-bond network (see Supporting Information, Figure S5). However, the conformation of STOP in 2H15 features a long N1–OG distance, not compatible with this interaction. The bifurcated H-bond coordination prompted us to analyze a second zwitterionic conformation (STOPZO, see Supporting Information, Figure S6). The energies derived from the conformational search in water solvent using the OPLS force field suggests an equilibrium between both zwitterion structures with the neutral conformer 60 kcal/mol higher in energy (see Supporting Information, Figure S6).

On the knowledge that the sulfamide analogue binds to CA II with the deprotonated sulfamide moiety coordinated to Zn, we ran 12 ns MD simulations for STOPN and STOPZ,

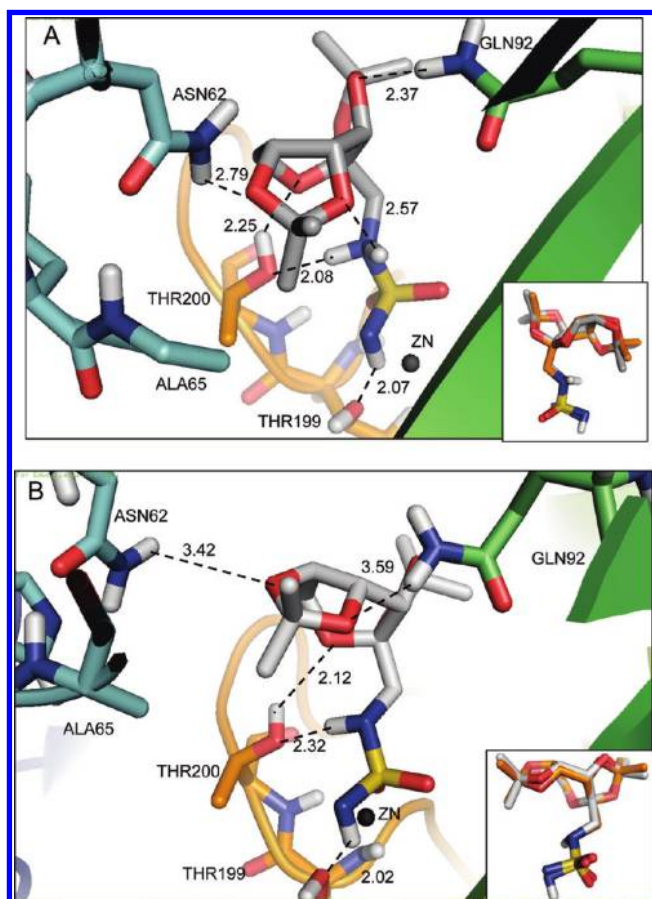


Figure 8. (A) Relevant interactions that stabilize STOPZ in the active site of CAII during the MD simulations. Average values are given. The superposition of one STOPZ representative MD snapshot and the crystallographic ligand are shown in the lower right corner. (B) Relevant interactions that stabilize STOPN in the active site of CAII during the MD simulations. Average values are given. The superposition of one STOPN representative MD snapshot and the crystallographic ligand are shown in the lower right corner.

starting from the X-ray structure (PDB code 2H15) for STOPN and modifying the ligand through protonation of the N for STOPZ.

The main H-bond interactions derived from the docking are conserved over the 12 ns MDs of CAII–STOPZ and CAII–STOPN. As in X-ray structure, the binder sulfamide function interacts with THR199 and THR 200, and the organic scaffold makes a network of H bonds with residues of the active site pocket in both cases (Figure 8A). In the case of STOPZ, the intramolecular N²–O₆ and N²–O₃ interactions are kept throughout the simulation. Conversely, the conformation of STOPN is only kept by the concerted N²–H–OG/OG–HG–O H-bond network, but the N²–endocyclic O₆ distance is longer (3.54 Å) at the end of the 12 ns MD than in the X-ray structure (3.2 Å), see Figure 8B. The slight relaxation of the structure impacts the interaction of the cap with the surrounding residues. A detailed comparison shows that only in the case of STOPZ the experimental interactions of the dioxolane O (O₅–GLN92 and O₇–ASN62) are conserved. As mentioned before, no water molecules were found in the active site of CAII during the MD, and only the organic scaffold (cap) of the ligand interacts with the solvent through the dioxolane O atoms.

The results obtained from docking, conformational analysis, and MD simulations are indicative of a strong influence

of H-bond interactions in the binding conformation of STOPZ, making STOPZ a better model than STOPN. The STOPZ model features a ligand with a protonated N² atom and a negative N¹. Accepting this model as closer to reality offers a possible interpretation of the unpredictable low inhibitory activity of STOP compared with other monosubstituted sulfamides, as the lack of a negative net charge in the ligand impairs its ability to interact with the positive Zn ion in the enzyme metalcenter.

The MD simulation of TOP-like confirms the prevalence of the positive interactions found in its X-ray structure. As described for STOP, no water molecules diffuse to the active site, and the cyclic sulfate O atoms of the cap are exposed to the solvent and form H bonds as predicted before considering crystallization waters¹⁶ (see Supporting Information, Figure S7).

CONCLUSION

The discovery of novel chemical entities as potent inhibitors and the origin of its activity at the molecular level are major goals in medicinal chemistry. In this line, understanding the effects that cause the lack of inhibition of new possible candidates represents equally valuable information for future inhibitor design. Through molecular modeling techniques supported by experimental data, we provided in this investigation an explanation for the different activity of sulfamides compared with their cognate sulfamates.

The analysis showed that the nature and the position of the sulfamide substituents as well the acidity and the ability of solvation of the sulfamide function directly impact the inhibitory capability. The results point to the importance of an organic scaffold (N- or O-substituent_{cap}) that maximizes interactions with hydrophobic and hydrophilic regions of the enzyme active site. In the design of the cap, intramolecular H bonds involving the N²H moiety should be avoided. Disubstitution, although increasing the number of possible interactions through the inclusion of a second substituent, has a negative effect on the inhibitory activity, as the substitution of the second sulfamide NH precludes the interaction with THR199.

Our results analyze the influence of solvation on the zinc-binding function of sulfamides and sulfamates and describe an interesting effect of H-bond coordination on intramolecular interactions that results in a formal decrease of the negative charge of N¹. However, an appropriate substitution that maximizes the positive interactions with the residues and increases the acidity of the N¹H can lead to interesting sulfamide inhibitors. As examples, we can mention arylsulfamides with an electron-withdrawing substituent in the aromatic ring,¹⁷ where the 4-(trifluoromethyl)phenylsulfamide ($K_i = 13$ nM), pentafluoromethylsulfamide ($K_i = 32$ nM), and 4-cyanophenylsulfamide ($K_i = 16$ nM) are more active than their cognate sulfamates.

ACKNOWLEDGMENT

L.E. Bruno Blanch is a member of the Facultad de Ciencias Exactas, Universidad Nacional de La Plata, and L. Gavernet is member of Consejo Nacional de Investigaciones Científicas y Técnicas de la República Argentina (CONICET). The work described herein was done in part during a Postdoctoral leave of Dr. L. Gavernet of the University of Notre Dame to whom

she gratefully acknowledges. This research was supported in part by the National Science Foundation (TG-CHE090124) through TeraGrid resources provided by NICS and LONI and by the Agencia de Promoción Científica y Tecnológica (PICT 00339/2007), CONICET, the Universidad Nacional de La Plata, Argentina, and the Walther Cancer Research Center, University of Notre Dame. The computations were performed on Kraken (a Cray XT5) at the National Institute for Computational Sciences (<http://www.nics.tennessee.edu/>) and on Queen Bee at the Louisiana Optical Network Initiative. Generous allocation of computing resources by the Center for Research Computing at the University of Notre Dame is also acknowledged. Work from CTS lab has been financed by an European Union grant of the seventh FP programme (Metoxia project).

Supporting Information Available: Additional figures that describe the interactions of the ligands in the CAII active site. This information is available free of charge via the Internet at <http://pubs.acs.org>

REFERENCES AND NOTES

- Lindskog, S.; Henderson, L. E.; Kannan, K. K.; Liljas, A.; Nyman, P. O.; Strandberg, B. Carbonic anhydrase. In *The Enzymes*, 3rd ed.; Boyer, P. D., Ed.; Academic Press: New York, 1971; Vol. 3, pp 587–665.
- Pocker, Y.; Saranen, S. Carbonic anhydrase: structure, catalytic versatility, and inhibition. *Adv. Enzymol. Relat. Areas Mol. Biol.* **1978**, *47*, 149–274.
- Sly, W. S.; Hu, P. Y. Human carbonic anhydrases and carbonic anhydrase deficiencies. *Annu. Rev. Biochem.* **1995**, *64*, 375–401.
- Supuran, C. T.; Scozzafava, A. Carbonic anhydrase inhibitors and their therapeutic potential. *Expert Opin. Ther. Pat.* **2000**, *10*, 575–600.
- Supuran, C. T.; Scozzafava, A.; Cassini, A. Carbonic anhydrase inhibitors. *Med. Res. Rev.* **2003**, *23*, 146–189.
- Pastorekova, S.; Parkkila, S.; Pastorek, J.; Supuran, C. T. Carbonic anhydrase: current state of the art, therapeutic applications and future prospects. *J. Enzyme Inhib. Med. Chem.* **2004**, *19*, 199–229.
- Supuran, C. T.; Scozzafava, A. Carbonic anhydrases as targets for medicinal chemistry. *Bioorg. Med. Chem.* **2007**, *15*, 4336–4350, and references cited therein.
- Hartsough, D. S.; Merz, K. M., Jr. Dynamic Force Field Models: Molecular Dynamics Simulations of Human Carbonic Anhydrase II Using a Quantum Mechanical/Molecular Mechanical Coupled Potential. *J. Phys. Chem.* **1995**, *99*, 11266–11275.
- Jackman, J. E.; Merz, K. M.; Fierke, C. A. Disruption of the active site solvent network in carbonic anhydrase II decreases the efficiency of proton transfer. *Biochemistry* **1996**, *35*, 16421–16428.
- Peng, Z.; Merz, K. M.; Banci, L. Binding of cyanide, cyanate, and thiocyanate to human carbonic anhydrase II. *Proteins* **1993**, *17*, 203–216.
- Rossi, K. A.; Merz, K. M.; Smith, G. M.; Baldwin, J. J. Application of the free energy perturbation method to human carbonic anhydrase II inhibitors. *J. Med. Chem.* **1995**, *38*, 2061–2069.
- Oltulu, O.; Yasar, M. M. Erolu, E.A QSAR study on relationship between structure of sulfonamides and their carbonic anhydrase inhibitory activity using the eigenvalue (EVA) method. *Eur. J. Med. Chem.* **2009**, *44*, 3439–3444.
- Eroglu, E.; Turkmen, H. A DFT-based quantum theoretic QSAR study of aromatic and heterocyclic sulfonamides as carbonic anhydrase inhibitors. *J. Mol. Graphics Modell.* **2007**, *26*, 701–708.
- Tuccinardi, T.; Nuti, E.; Ortore, G.; Supuran, C. T.; Rossello, A.; Martinelli, A. Analysis of Human Carbonic Anhydrase II: Docking Reliability and Receptor-Based 3D-QSAR Study. *J. Chem. Inf. Model.* **2007**, *47*, 515–525.
- Singh, J.; Shaik, B.; Singh, S.; Sikhima, S.; Agrawal, V. K.; Khadikar, P. V.; Supuran, C. T. QSAR studies on the activation of the human carbonic anhydrase cytosolic isoforms I and II and secretory isozyme VI with amino acids and amines. *Bioorg. Med. Chem.* **2007**, *15*, 6501–9.
- Winum, J. Y.; Temperini, C.; El Cheikh, K.; Innocenti, A.; Vullo, D.; Ciattini, S.; Montero, J. L.; Scozzafava, A.; Supuran, C. T. Carbonic Anhydrase Inhibitors: Clash with Ala65 as a Means for Designing Inhibitors with Low Affinity for the Ubiquitous Isozyme II, Exemplified by the Crystal Structure of the Topiramate Sulfamide Analogue. *J. Med. Chem.* **2006**, *49*, 7024–7031.
- Casini, A.; Winum, J.-Y.; Montero, J.-L.; Scozzafava, A.; Supuran, C. T. Carbonic anhydrase inhibitors: inhibition of cytosolic isozymes I and II with sulfamide derivatives. *Bioorg. Med. Chem. Lett.* **2003**, *13*, 837–840.
- Gavernet, L.; Dominguez Cabrera, J.; Bruno Blanch, L.; Estiú, G. 3D-QSAR design of novel antiepileptic sulfamides. *Bioorg. Med. Chem.* **2007**, *15*, 1556–1567.
- Gavernet, L.; Barrios, I.; Sella Cravero, M.; Bruno Blanch, L. Design, synthesis, and anticonvulsant activity of some sulfamides. *Bioorg. Med. Chem.* **2007**, *15*, 5604–5614.
- Barrios, I. A.; Rocha Arrieta, L.; Bruno-Blanch, L. E. Unpublished results.
- Khalifah, R. G. The carbon dioxide hydration activity of carbonic anhydrase. I. Stop-flow kinetic studies on the native human isoenzymes B and C. *J. Biol. Chem.* **1971**, *246*, 2561–2573.
- Innocenti, A.; Vullo, D.; Pastorek, J.; Scozzafava, A.; Pastorekova, S.; Nishimori, I.; Supuran, C. T. Carbonic anhydrase inhibitors. Inhibition of transmembrane isozymes XII (cancer-associated) and XIV with anions. *Bioorg. Med. Chem. Lett.* **2007**, *17*, 1532–1537.
- Supuran, C. T. Carbonic anhydrases: novel therapeutic applications for inhibitors and activators. *Nat. Rev. Drug Discovery* **2008**, *7*, 168–181.
- Morris, G. M.; Goodsell, D. S.; Halliday, R. S.; Huey, R.; Hart, W. E.; Belew, R. K.; Olson, A. J. Automated Docking Using a Lamarckian Genetic Algorithm and an Empirical Binding Free Energy Function. *J. Comput. Chem.* **1998**, 1639–1662.
- Jude, K. M.; Banerjee, A. L.; Haldar, M. K.; Manokaran, S.; Roy, B.; Mallik, S.; Srivastava, D. K.; Christianson, D. W. Ultrahigh Resolution Crystal Structures of Human Carbonic Anhydrases I and II Complexed with “Two-Prong” Inhibitors Reveal the Molecular Basis of High Affinity. *J. Am. Chem. Soc.* **2006**, *128*, 3011–3018.
- Schafmeister, C.; Ross, W. S.; Romanovski, V. *LEaP*; University of California: San Francisco, 1995.
- Quality Atomic Charges, Proton Assignment and Canonicalization, QuACPAC*; OpenEye Scientific Software, Inc.: Santa Fe, NM, 2007.
- Mohamadi, F.; Richards, N. G.; Guida, W. C.; Liskamp, R.; Lipton, M.; Caufiel, C.; Chang, G.; Hendrickson, T.; Still, W. C. MacroModel: An Integrated Software System for Modeling Organic and Bioorganic Molecules Using Molecular Mechanics. *J. Comput. Chem.* **1990**, *11*, 440–467.
- Jorgensen, W. L.; Tirado-Rives, J. Potential energy functions for atomic-level simulations of water and organic and biomolecular systems. *Proc. Natl. Acad. Sci. U.S.A.* **2005**, *102*, 6665–6670.
- Shenkin, P. S.; McDonald, D. Q. Cluster Analysis of Molecular Conformations. *J. Comput. Chem.* **1994**, *15*, 899–916.
- Case, D. A.; Darden, T. A.; Cheatham, I. T. E.; Simmerling, C. L.; Wang, J.; Duke, R. E.; Luo, R.; Crowley, M.; Walker, R. C.; Zhang, W.; Merz, K. M. J.; Wang, B.; Hayik, S.; Roitberg, A.; Seabra, G.; Kolossvary, I.; Wong, K. F.; Paesani, F.; Vanicek, J.; Wu, X.; Brozell, S.; Steinbrecher, H.; Gohlke, H.; Yang, L.; Tan, C.; Mongan, J.; Hornak, V.; Cui, G.; Mathews, D. H.; Seetin, M. G.; Sagui, C.; Babin, V.; Kollman, P. A. *AMBER 10*; University of California: San Francisco, CA, 2008.
- Jorgensen, W. L. C. J.; Madura, J.; Impey, R. W.; Klein, M. L. Comparison of simple potential functions for the simulation of liquid water. *J. Chem. Phys.* **1983**, *79*, 926–935.
- Wang, J.; Wolf, R. M.; Caldwell, J. W.; Kollman, P. A.; Case, D. A. Development and testing of a general AMBER force field. *J. Comput. Chem.* **2004**, *25*, 1157–1174.
- Bayly, C. A.; Cieplak, P.; Cornell, W. D.; Kollman, P. A. A well behaved electrostatic potential based method using charge restraints for deriving atomic charges: The RESP model. *J. Phys. Chem.* **1993**, *97*, 10269–10280.
- Fox, T.; Kollman, P. A. Application of RESP Methodology in the Parametrization of Organic Solvents. *J. Phys. Chem. B* **1998**, *102*, 8070–8079.
- Becke, A. D.; Yarkony, D. R. In *Modern Electronic Structure Theory Part II*; World Scientific: Singapore, 1995.
- Frisch, M. J.; Trucks, G. W.; Schlegel, H. B.; Scuseria, G. E.; Robb, M. A.; Cheeseman, J. R.; Montgomery, J. A., Jr.; Vreven, T.; Kudin, K. N.; Burant, J. C.; Millam, J. M.; Iyengar, S. S.; Tomasi, J.; Barone, V.; Mennucci, B.; Cossi, M.; Scalmani, G.; Rega, N.; Petersson, G. A.; Nakatsuji, H.; Hada, M.; Ehara, M.; Toyota, K.; Fukuda, R.; Hasegawa, J.; Ishida, M.; Nakajima, T.; Honda, Y.; Kitao, O.; Nakai, H.; Klene, M.; Li, X.; Knox, J. E.; Hratchian, H. P.; Cross, J. B.; Bakken, V.; Adamo, C.; Jaramillo, J.; Gomperts, R.; Stratmann, R. E.; Yazyev, O.; Austin, A. J.; Cammi, R.; Pomelli, C.; Ochterski, J. W.; Ayala, P. Y.; Morokuma, K.; Voth, G. A.; Salvador, P.; Dannenberg, J. J.; Zakrzewski, V. G.; Dapprich, S.; Daniels, A. D.; Strain, M. C.; Farkas, O.; Malick, D. K.; Rabuck, A. D.; Raghavachari, K.; Foresman, J. B.;

- Ortiz, J. V.; Cui, Q.; Baboul, A. G.; Clifford, S.; Cioslowski, J.; Stefanov, B. B.; Liu, G.; Liashenko, A.; Piskorz, P.; Komaromi, I.; Martin, R. L.; Fox, D. J.; Keith, T.; Al-Laham, M. A.; Peng, C. Y.; Nanayakkara, A.; Challacombe, M.; Gill, P. M. W.; Johnson, B.; Chen, W.; Wong, M. W.; Gonzalez, C.; Pople, J. A. *Gaussian 03*, revision C.02; Gaussian, Inc.: Wallingford, CT, 2004.
- (38) Ryckaert, J. P.; Ciccotti, G.; Berendsen, H. J. C. Numerical integration of the cartesian equations of motion of a system with constraints: Molecular dynamics of n-alkanes. *J. Comput. Phys.* **1977**, *23*, 327–341.
- (39) Pastor, R. W.; Brooks, B. R.; Szabo, A. An analysis of the accuracy of Langevin and molecular dynamics algorithms. *Mol. Phys.* **1988**, *65*, 1409–1419.
- (40) Petersen, H. G. Accuracy and efficiency of the particle-mesh-ewald method. *J. Chem. Phys.* **1995**, *103*, 3668–3679.
- (41) Essman, V.; Perera, L.; Berkowitz, M. L.; Darden, T.; Lee, H.; Pedersen, L. G. A smooth particle-mesh-Ewald method. *J. Chem. Phys.* **1995**, *103*, 8577–8593.
- (42) Winum, J. Y.; Vullo, D.; Casini, A.; Montero, J. L.; Scozzafava, A.; Supuran, C. T. Carbonic Anhydrase Inhibitors. Inhibition of Cytosolic Isozymes I and II and Transmembrane, Tumor-Associated Isozyme IX with Sulfamates Including EMATE Also Acting as Steroid Sulfatase Inhibitors. *J. Med. Chem.* **2003**, *46*, 2197–2204.
- (43) Winum, J. Y.; Vullo, D.; Casini, A.; Montero, J. L.; Scozzafava, A.; Supuran, C. T. Carbonic Anhydrase Inhibitors: Inhibition of Transmembrane, Tumor-Associated Isozyme IX, and Cytosolic Isozymes I and II with Aliphatic Sulfamates. *J. Med. Chem.* **2003**, *46*, 5471–5477.
- (44) Vitale, R. M.; Alterio, V.; Innocenti, A.; Winum, J. Y.; Monti, S. M.; De Simone, G.; Supuran, C. T. Carbonic Anhydrase Inhibitors. Comparison of Aliphatic Sulfamate/Bis-sulfamate Adducts with Isozymes II and IX as a Platform for Designing Tight-Binding, More Isoform-Selective Inhibitors. *J. Med. Chem.* **2009**, *52*, 5990–5998.

CII00112S